IEEE International Conference on Robotics and Automation, Atlanta, GA, May 1993, Vol. 2, pp. 130-135,

2-D Contact Detection and Localization Using Proprioceptive Information*

Roderic A. Grupen and Manfred Huber
Laboratory for Perceptual Robotics
Department of Computer Science
University of Massachusetts, Amherst MA 01003

Abstract

Knowledge of contact properties is important to interact with an unknown object in the environment. This paper presents a method to provide this information for a planar manipulator using general motions and the readings of joint angle and torque sensors and requires therefore no complex hardware like tactile sensor arrays. In a first stage, the algorithm combines geometric evidence of the instantaneous center and a term for the intersection with the previous link postures in a filter to obtain a hypothesis of the contact location on the link. Then torque domain evidence is used to verify this position estimate. Using this scheme, the algorithm can detect the contact location, surface normal and an estimate of the contact force for each link.

1 Introduction

In order to perform dextrous manipulation of unknown objects it is essential to have information about the interaction between the manipulator and the environment. This data in form of the locations, normals and forces of the existing contacts can be provided by tactile sensing and then be used for such different tasks as force control of whole-arm manipulators [2], incremental grasp configuration [3] or object recognition [1].

Most of the work on tactile perception has focused on the use of tactile sensor arrays (see [5] for an overview) in order to gather this information. This approach, however, requires the distribution of many "taxels" all over the manipulator resulting in packaging problems and changed characteristics of the robot arm. A second path using the readily available proprioceptive information (joint angles, velocities and torques) promises to avoid these difficulties. Several methods for this have been proposed, all of which require motion control to either avoid dynamic effects for the ones using only torque [2] or force sensor readings [6], or to initiate self posture changing motions (spcm) in the intersection based algorithm of [4]. The approach taken in this paper avoids this interference in the robot control by employing general motions of the manipulator and rigid body constraints to estimate contact properties. This problem is tackled by combining the evidence of three different observations into a final contact hypothesis.

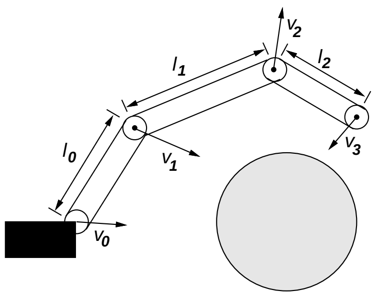

Figure 1: Planar Robot Arm with Spherical Object

Figure 1 shows a three link planar manipulator with revolute joints and some of the variables used throughout this paper, the most important of which are

Θ_i^t , $\dot{\Theta}_i^t$	Joint angle and velocity
τ_i^t	Joint torque
l_i , r_i	Link length and radius
v_i^t	Cartesian velocity of joint axis
$p_i^t = \begin{pmatrix} x_i^t \\ y_i^t \end{pmatrix}$	Cartesian location of joint axis
P^t	Link Posture ,

where subscript i indicates the link/joint number and superscript t the time of the observation[1].

*This work was supported in part by NSF IRI-9116297, CDA-8922572 and IRI-9208920

[1]Subscripts and superscripts are avoided wherever possible to simplify the corresponding equations

In the following, Sections 2 and 3 discuss the localization phase, which uses geometric observations to obtain estimates of the contact locations, and the torque based detection part, respectively. Section 4, finally, shows some data obtained for a geometric modeling task using a dynamic robot simulator and the fingers of a Utah/MIT hand.

2 Contact Localization

In the contact localization phase, two geometric observations are combined in a filter in order to obtain an estimate of hypothetical contact positions and surface normals. Because of the different geometry of the parallel link surfaces and the spherical tip regions, these have to be treated separately.

2.1 Link Contacts

For the link, the location of a contact point is given by the distance d from the proximal joint to the contact along the link axis, and the side s, given by 1 for the left and -1 for the right side of the link which is found by means of joint torque information in Section 3. Using this internal representation, constraints on the movements of the manipulator can be found which determine a possible contact location on a link by link basis.

2.1.1 Posture Intersection

As noted in [4], the intersection of two consecutive postures gives an estimate of the contact location. In this paper, however, a corrected term for the intersection point of the link axis is used. The distance k^t of this point for the two postures P^{t-1} and P^t from the proximal endpoint at time t is given by

$$k^t = l \frac{\Delta y_1 {\ell_x}^{t-1} - \Delta x_1 {\ell_y}^{t-1}}{{\ell_x}^t {\ell_y}^{t-1} - {\ell_y}^t {\ell_x}^{t-1}} \;, \tag{1}$$

where $\ell_x^t = x_2^t - x_1^t$.

This location k, however, is not the precise position of the contact point and therefore a correction term δ_k for this has to be found. Assuming constant curvature of the object surface between two posture recordings, analysis of the relations shown in Figure 2 leads to a value for this term of

$$\delta_k = \left(\frac{b}{\varphi} + r\right) \tan\frac{\varphi}{2} \;. \tag{2}$$

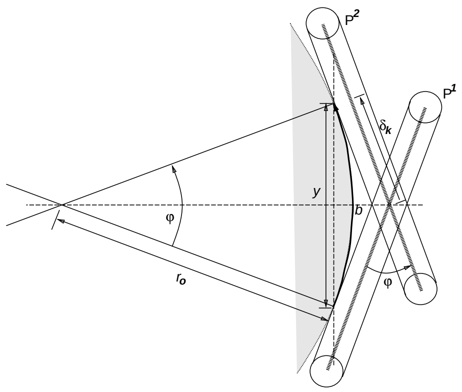

Figure 2: Correction of Intersection Point

where b denotes the distance the contact traveled on the object. This together with Equation 1 results in a location estimate

$$d' = k + \delta_k \;. \tag{3}$$

2.1.2 Instantaneous Center

Any planar motion of a planar rigid body is equivalent to a pure rotation about an instantaneous center. The construction of this point for a link of the used robot is given by the intersection of the normals of the two Cartesian velocity vectors in the link endpoints.

In the absence of slip, this point coincides with the contact location but slip moves the center away from the link surface.

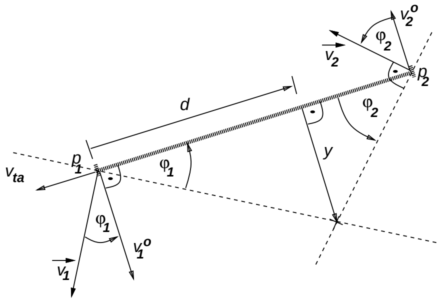

Figure 3: Instant Center for Contact with Slip

Examining the properties of Figure 3 leads to the functions

$$d = l \frac{v_1^o}{v_1^o - v_2^o} \;, \quad y = l \frac{v_{ta}}{v_2^o - v_1^o} \tag{4}$$

for the location of the instantaneous center, where v_{ta} and v^o denote the tangential and orthogonal components of the velocity vectors, respectively.

This means, that, in the presence of a contact, besides establishing the location d of the contact point, the position of the center also determines the slip velocity.

2.1.3 Position Filtering

The integration of the new observation d of the previous section at time t is done using contact tracking in a linear observer. Employing error estimates ε instead of variances in the equations of this discrete Kalman filter results in the equations

$$\begin{aligned} \hat{d}^t &= \left(\hat{d}^{t-1} + v_c \Delta t\right) + K^t \left(d - \left(\hat{d}^{t-1} + v_c \Delta t\right)\right) \\ \hat{\varepsilon}^t &= \varepsilon_d K^t \\ K^t &= \frac{\hat{\varepsilon}^{t-1} + \varepsilon_{v_c} \Delta t}{\varepsilon_d + \hat{\varepsilon}^{t-1} + \varepsilon_{v_c} \Delta t} \end{aligned} \tag{5}$$

with

$\hat{d}^t$ = Filtered location at time t
d = Location hypothesis of Equation 4
v_c = Contact point velocity on the link
$\hat{\varepsilon}^t$ = Uncertainty associated with $\hat{d}^t$
ε_d = Uncertainty associated with d
ε_{v_c} = Uncertainty associated with v_c .

In order to use this observer, however, values for the unknown variables v_c, ε_{v_c} and ε_d have to be found. For the former two, a filtered version of $\frac{\Delta \hat{d}}{\Delta t}$ and $\frac{\hat{\varepsilon}^t + \hat{\varepsilon}^{t-1}}{\Delta t}$ can be used. The derivation of an estimate for the latter, using the intersection hypothesis d' as a second observer, is shown in the next section.

2.1.4 Error Analysis

To utilize the intersection term of Equation 3, a value for the unknown variable b must be determined. This can be derived from the relation

$$(b + d_s) \cong \left(d - \hat{d}^{t-1}\right) ,$$

where

b = Distance due to rolling
$d_s \approx \frac{v_s^t + v_s^{t-1}}{2} \Delta t$ = Distance due to slip
v_s^t = Slip velocity

assuming a constant slip acceleration between two observations.

Using this for the intersection estimate and performing a worst case error analysis with Equations 2 and 3 results in

$$\varepsilon_d \leq \frac{\hat{\varepsilon}^{t-1} \frac{1}{\varphi} \tan \frac{\varphi}{2} + \left| d' - d \right|}{1 - \frac{1}{\varphi} \tan \frac{\varphi}{2}} \quad \text{for } \frac{\tan \frac{\varphi}{2}}{\varphi} < 1 \tag{6}$$

as a bounded error in the contact location. This term can now be used in Equation 5 to compute the final estimate of the contact location $\hat{d}^t$.

2.2 Tip Contacts

In the following, contact locations on the spherical tip and knuckle regions of the manipulator are represented by the angle ϕ towards the surface normal in the point of contact.

2.2.1 Location from Velocity

In the presence of a tip contact, all Cartesian velocity is tangential to the object surface in the point of contact. Therefore, the contact location ϕ is perpendicular to the endpoint velocity,

$$\begin{pmatrix} \cos \phi \\ \sin \phi \end{pmatrix} = \pm \frac{1}{||v||} \begin{pmatrix} -v_y \\ v_x \end{pmatrix} , \tag{7}$$

which leaves two possible points for a full sphere but since the tip is only a hemisphere, only one of the solutions remains.

2.2.2 Location from Displacement

In the same way, the displacement Δp of the endpoint for two consecutive postures can be used to get an estimate ψ of the contact location, where

$$\begin{pmatrix} \cos \psi \\ \sin \psi \end{pmatrix} = \pm \frac{1}{||\Delta p||} \begin{pmatrix} -\Delta y \\ \Delta x \end{pmatrix} . \tag{8}$$

This position, however, is only an approximation which depends on the curvature of the object, requiring a correction term to obtain the precise location.

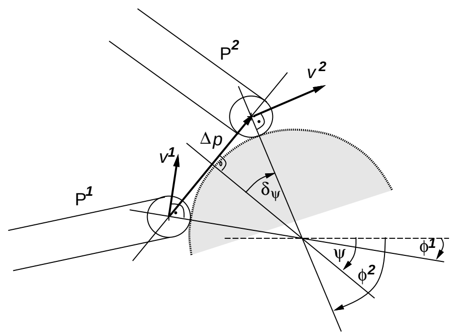

Figure 4: Correction for Displacement Based Point

Under the assumption of a constant curvature between two consecutive observations, the properties shown in Figure 4 lead to the expression δ_ψ for this term as

$$\delta_\psi = \frac{1}{2} \left(\phi^2 - \phi^1\right) \tag{9}$$

and therefore the corrected angular representation of the contact is

$$\phi' = \psi + \delta_\psi . \tag{10}$$

2.2.3 Position Filtering

In the same way as for the links, a linear observer is used to track the contact point across the tip surface and to integrate new observations. Replacing the variances in the Kalman filter equations again with error estimates ϵ results in

$$\begin{aligned}
\hat{\phi}^t &= \left(\hat{\phi}^{t-1} + \omega \Delta t\right) + K^t \left(\phi - \left(\hat{\phi}^{t-1} + \omega \Delta t\right)\right) \\
\hat{\epsilon}^t &= \epsilon_\phi K^t \\
K^t &= \tfrac{\hat{\epsilon}^{t-1} + \epsilon_\omega \Delta t}{\epsilon_\phi + \hat{\epsilon}^{t-1} + \epsilon_\omega \Delta t} \ ,
\end{aligned} \tag{11}$$

where

$\hat{\phi}^t$ = Filtered location at time t
ϕ = Location hypothesis of Equation 7
ω = Angular contact point velocity
$\hat{\epsilon}^t$ = Uncertainty associated with $\hat{\phi}^t$
ϵ_ϕ = Uncertainty associated with ϕ
ϵ_ω = Uncertainty associated with ω

for this filter. The variables ω and ϵ_ω can be approximated by $\frac{\Delta \hat{\phi}}{\Delta t}$ and $\frac{\hat{\epsilon}^t + \hat{\epsilon}^{t-1}}{\Delta t}$. To determine the remaining unknown ϵ_ϕ, the displacement based hypothesis ϕ' of Equation 10 is used, leading to the considerations of the next section.

2.2.4 Error Analysis

Using $\hat{\epsilon}^{t-1}$ as the worst case error of the previous contact estimate in Equations 9 and 10 leads to the term

$$\epsilon_\phi \leq \hat{\epsilon}^{t-1} + 2 \left|\phi' - \phi\right| \tag{12}$$

for the worst case error which can be used in the filter of Equation 11.

2.3 Link-Tip Decision

The localization part of the previous sections results in two location estimates per link of the manipulator (one on the link and one on the tip surface). It is therefore necessary to make a decision for either one of these which is done by means of additional constraints on the positions and movements of the contact point [2].

2.3.1 Constraints on Link Contacts

Since the location estimate for link contacts is based on the instantaneous center of rotation, many situations with a tip contact result in a hypothesis outside the actual link surface (i.e. $\hat{d} < 0 \ \vee \ \hat{d} > l$). Putting this in relation to the uncertainty associated with this location, a measure of evidence $E_{\hat{d}}^-$ against a link contact can be formed as

$$E_{\hat{d}}^- = \begin{cases} \frac{\hat{d}-l}{\hat{\epsilon}} & \text{for } \hat{d} > l \\ \frac{-\hat{d}}{\hat{\epsilon}} & \text{for } \hat{d} < 0 \\ 0 & \text{otherwise} \ . \end{cases} \tag{13}$$

In a similar way, limitations on the motions of a contact on the link can be found, leading to a second term $E_{v_c}^-$ of counterevidence for link contacts

$$E_{v_c}^- = \frac{\max\left(0, \ -s \cdot sign\left(\dot{\theta}\right)(v_c - v_s)\right)}{\varepsilon_{v_c}} \ , \tag{14}$$

where

$v_c \ , \ v_s$ = Contact and slip velocity
s = Contact side of the link
$\dot{\theta}_i = \left(\sum_{j=0}^{i} \dot{\Theta}_j\right)$ = Rotational vel. of link i .

2.3.2 Constraints on Tip Contacts

Since the decision for the side s is torque based, it also applies to the tip region and decides on which side of the link axis the contact exists. Using this, the location $\hat{\phi}$ of the contact can be tested and evidence $E_{\hat{\phi}}^-$, this time against the existence of the hypothesized tip contact, can be found as

$$E_{\hat{\phi}}^- = \frac{\max\left(0, \ -s\left(\hat{\phi} - \theta\right)\right)}{\hat{\epsilon}} \ , \tag{15}$$

where

$\theta_i = \sum_{j=0}^{i} \Theta$ = Orientation of link i
$\left(\hat{\phi} - \theta\right)$ scaled between $-\pi$ and π .

The term used for the experiments in Section 4, for example, is the simple linear combination

$$sign\left(0.5 + E_{\hat{\phi}}^- - E_{\hat{d}}^- - E_{v_c}^-\right) \ ,$$

where 1 denotes link and -1 tip contact.

3 Contact Detection

The preceding sections use kinematic constraints to hypothesize contact locations under the assumption that a contact exists. Since, however, all motions can be simulated in the absence of any interaction with

[2] These constraints, however, can not find the correct solution in every case because of the possible equivalence of motions with different contact configurations.

the environment, these geometric properties can not decide the existence of a contact and thus additional information has to be used to verify the estimates. To avoid the necessity of strategic posture changes, torque domain evidence is used here.

3.1 Force Calculation

Assuming that all measured torques are due to interactions with the environment (i.e. no dynamic effects are present), the side information s can be simply found as

$$s = sign\,(\tau) \tag{16}$$

because of the relation between the contact force and the torque in this joint. For the derivation of the magnitude of the force for a frictionless contact from the torque of the proximal joint of this link, some additional considerations are necessary as illustrated in Figure 5.

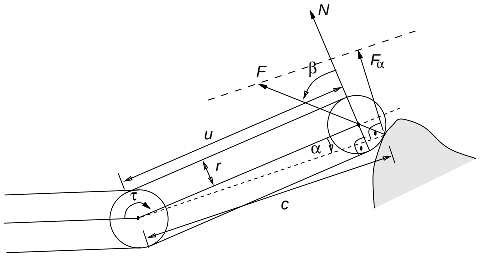

Figure 5: Contact Force Construction

Using these properties, the contact force F can be calculated by

$$|F| = \frac{|F_\alpha|}{\cos(\alpha+\beta)} = \frac{|\tau|}{c\cdot\cos(\alpha+\beta)} \tag{17}$$

for a point contact without friction, where

$$\left.\begin{array}{ll} u & = \hat{d} \\ \beta & = (s+1)\,\frac{\pi}{2} \end{array}\right\}\ \text{for link contacts}$$
$$\left.\begin{array}{ll} u & = l \\ \beta & = \frac{\pi}{2} + \hat{\phi} - \sum_{j=0}^{i}\Theta_j \end{array}\right\}\ \text{for tip contacts .}$$

3.2 Torque Decomposition

Since all motions of a robot manipulator cause dynamic torques, these have to be compensated in order to be able to compute the correct contact forces. For a real robot, however, no perfect model of the dynamics is available and worst cases are used here to obtain an interval of possible torque values[3]. Starting from the most distal link, the existence of a contact is then confirmed if the measured torques are outside this interval, integrating the extrema of the torques due to the detected contact into the interval. Using this worst case approach which allows to integrate different kinds of uncertainties, multiple contacts on different links together with the contact forces can be estimated.

[3] In most situations only good inertial parameters are required because the contact localization can be expected to occur during low velocity movements.

3.3 Friction

Coulomb friction can be seen as a pure uncertainty in the direction of the contact force, represented by the friction cone (or half the cone if the direction of slip is known). The only changes occur therefore in the possible contact force. This, however, can be easily derived from Equation 17 as

$$|F| = \frac{|\tau|}{c\cdot\cos(\alpha+\beta\pm\vartheta)}\ , \tag{18}$$

where

$$\tan\vartheta = \mu_f = \text{ maximum coefficient of friction .}$$

4 Experiments

4.1 Simulation Results

This section presents performance results obtained from a dynamic robot simulator, modeling the object surface as a spring. Figure 6 shows a sequence of snapshots of the manipulator and the estimated contact locations as circles, where the radius denotes the associated uncertainty. For these experiments, the manipulator was moved with a constant speed of $0.33m/s$ from right to left, while compliance was achieved by means of a PD-controller using reference angles $\Theta_{ref_i} = \pi/4$. Figure 7 presents the probability distribution of the absolute distance between the estimate and the object surface. This data shows only one point outside the object while all the others are up to $0.6mm$ inside (recall that this is an elastic object and the manipulator has to push on it to observe it).

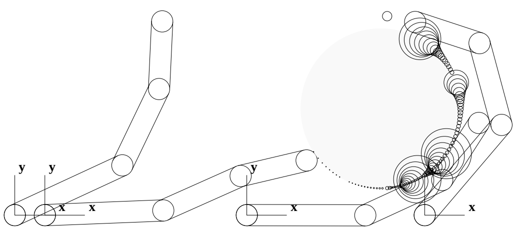

Figure 6: Contacts for Circular Object

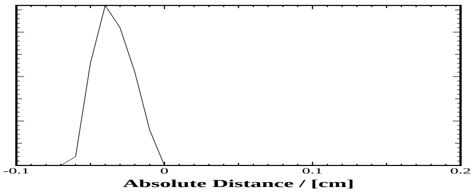

Total Outliers : 0.8%

Figure 7: Absolute Distance Error

4.2 Robot Results

To confirm the applicability of the algorithm on a real robot, similar experiments were performed using the thumb and index finger of a Utah/MIT dextrous hand mounted on a GE P50 robot. Compliance of the fingers was achieved by means of a PD controller and constant reference angles Θ_{ref} while the robot moved the hand along a straight path. The object in form of a hexagonal peg was held in place by the gripper of a second P50 manipulator. Figure 8 shows the setup

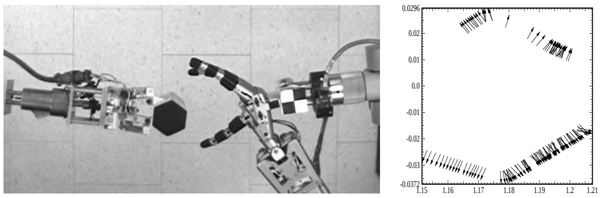

Figure 8: Contact Points and Normals for Hexagon

on the left and the raw output data in form of contact points with surface normals on the right.

5 Conclusions and Future Work

Using only joint angle and torque sensors, this algorithm allows to gather contact data while interacting with an unknown object in the environment, without restricting the motions of the robot. It can therefore be used for all tasks requiring contact information.

One of the remaining problems is how to combine the tactile information with other sensory information (e.g. vision). One way under investigated here involves Hough accumulator arrays to incrementally build a model. Figure 9 and 10 show density plots of accumulators obtained by special purpose vision, modeling the black hexagon on a white background, and haptic information, respectively (the dark regions are peaks, representing an edge of the model).

A second goal for future work is the extension of this approach into 3D.

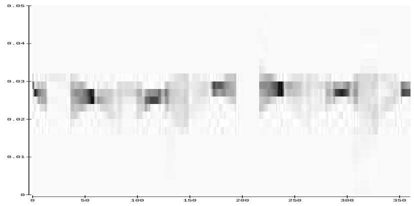

Figure 9: Hough Accumulator for Hexagon

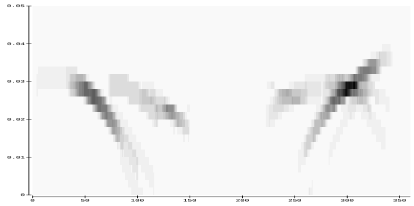

Figure 10: Haptic Accumulator for Hexagon

References

[1] P.K. Allen. Integrating vision and touch for object recognition tasks. *International Journal of Robotics Research*, 7(6):15–33, 1988.

[2] S.J. Gordon and W.T. Townsend. Integration of tactile-force and joint-torque information in a whole-arm manipulator. In *Proceedings of the IEEE International Conference on Robotics and Automation*, pages 464–469, Scottsdale, AZ, May 1989. IEEE.

[3] R.A. Grupen. Planning grasp strategies for multifingered robot hands. In *Proceedings of the IEEE International Conference on Robotics and Automation*, pages 646–651, Sacramento, CA, April 1991. IEEE.

[4] M. Kaneko and K. Tanie. Contact point detection for grasping of an unknown object using self-posture changeability (spc). In *Proceedings of the IEEE International Conference on Robotics and Automation*, pages 864–869, Cincinnati, OH, May 1990. IEEE.

[5] H.R. Nicholls and M.H. Lee. A survey of robot tactile sensing technology. *International Journal of Robotics Research*, 8(3):3–30, 1989.

[6] T. Tsujimura and T. Yabuta. A tactile sensing method employing force/torque information through insensitive probes. In *Proceedings of the IEEE International Conference on Robotics and Automation*, pages 1315–1320, Nice, France, May 1992. IEEE.